International Immunopharmacology 69 (2019) 202–212

Contents lists available at ScienceDirect

International Immunopharmacology

journal homepage: www.elsevier.com/locate/intimp

Morphological and functional analysis of beige (Chèdiak-Higashi syndrome) mouse mast cells with giant granules

Takeshi Kiyoi[a,b], Shuang Liu[b], Muhammad Novrizal Abdi Sahid[b], Masachika Shudou[a], Masahito Ogasawara[c], Masaki Mogi[b,*], Kazutaka Maeyama[b]

[a] Division of Analytical Bio-medicine, Advanced Research Support Center, Ehime University, Shitsukawa, Toon, Ehime 791-0295, Japan
[b] Department of Pharmacology, Ehime University Graduate School of Medicine Shitsukawa, Toon, Ehime 791-0295, Japan
[c] Department of Pathogenesis and Control of Oral Diseases, Division of Dental Pharmacology, Iwate Medical University School of Dentistry, Morioka, Iwate 020-8505, Japan

A B S T R A C T

Chèdiak-Higashi syndrome is a rare autosomal recessive disease that causes hypopigmentation, recurrent infections, mild coagulation defects and neurological problems. Beige mice carry a mutation in the *lysosome trafficking regulator* (*LYST*) gene and display some of the key characteristics of human Chèdiak-Higashi syndrome, in particular, a high susceptibility to infection due to aberrant natural killer (NK) cell and polymorphonuclear leucocyte function. Morphological analysis of beige mice reveals the presence of enlarged lysosomes in a variety of cell types, including leucocytes, hepatocytes, fibroblasts and renal tubule cells. To examine the process of granule maturation and degranulation in beige mice mast cells, morphological studies have been conducted using a combination of electrophysiological techniques; however, few functional studies have been conducted with mast cells, such as mediator release. The aim of the present study was to determine the morphological and functional characteristics of skin and peritoneal mast cells and bone marrow-derived mast cells of homozygous (*bg/bg*) and heterozygous (*bg/+*) beige mice and wild-type (*+/+*) mice. The histamine concentration was lower in the peritoneal and bone marrow-derived mast cells of *bg/bg* mice compared with those of *bg/+* and *+/+* mice, but the histamine release response was potentiated. In vivo studies of passive cutaneous anaphylaxis showed no differences between *bg/bg* mice and either *bg/+* or *+/+* mice. Although *bg/bg* mast cells with enlarged granules display specific exocytotic processes in vitro, the consequences of mast cell activation in beige mice were similar to those of wild-type mice in vivo.

1. Introduction

Chèdiak-Higashi syndrome (CHS) is a rare autosomal recessive genetic disorder, which manifests as partial albinism, abnormally enlarged granules in various cell types, mild coagulation defects and neurological problems [1,2]. Susceptibility to infection is mainly due to polymorphonuclear leucocyte dysfunction, such as impaired phagolysosomes and chemotaxis [3].

The beige mouse and rat are established animal models for CHS because their phenotype and pathophysiology are extremely similar to those of human CHS [4]. Human CHS is caused by a mutation in the *CHS1/lysosomal trafficking regulator* (*LYST*) gene, the human orthologue of the mouse *LYST* gene [5]. LYST is a member of the beige and Chèdiak-Higashi (BEACH) family and interacts with proteins that are important for vesicular transport and signal transduction, including soluble *N*-ethylmaleimide sensitive factor attachment protein receptors (SNARE)-complex proteins, hepatocyte growth factor–regulated tyrosine kinase substrate (HRS), 14-3-3, and casein kinase 2 [6], and regulates lysosome size by affecting cell fission [7]. Protein kinase C (PKC) activity is downregulated in polymorphonuclear cells, NK cells, and fibroblasts isolated from beige mice [8–11].

Mast cells play a role in acute allergic inflammation, modulating the release of histamine and other chemical mediators [12]. In beige mice, enlarged granules are observed within mast cells [13–15]. It was reported that the peritoneal mast cells (PMCs) of beige mice undergo exocytotic degranulation following stimuli from either IgE-mediated antigens or degranulation agents [16,17]. Exocytotic degranulation due to IgE-mediated antigen stimulation has also been demonstrated in bone marrow-derived mast cells (BMMCs) from beige mice [18]. On the other hand, enlarged granules from beige mice have been used as tools to examine cell transplantation and as markers of exocytosis using morphological and electrophysiological techniques. Kitamura et al. found that mast cells are derived from bone marrow stem cells, not from connective tissue origin, by transplanting beige mouse bone marrow cells into congenic mice; it was easy to recognize the beige mice mast cells due to their larger sized granules than normal mast cells [19,20].

Although it was previously reported that histamine release in beige rat PMCs is abnormally enhanced [21], few studies have examined the function of beige mouse mast cells. Beige mice with a mutation of the

* Corresponding author.
E-mail address: mmogi@m.ehime-u.ac.jp (M. Mogi).

https://doi.org/10.1016/j.intimp.2019.01.053
Received 18 January 2019; Accepted 30 January 2019
Available online 06 February 2019

LYST/BEACH gene show faint skin colour and are easily discriminated from congenic wild-type mice, but no reports have shown the phenotype of mast cells from heterozygote (*bg/+*) mice with concurrent genotyping. Therefore, we sought to confirm the mutation of the *LYST* gene in homozygote and heterozygote beige strains accompanied by morphological and functional studies of mast cells. In the present study, morphological and functional analyses were performed using skin mast cells and PMCs, BMMCs of C57BL/6-+/+, *-bg/+*, *-bg/bg* mice, with a particular focus on histamine concentrations and release. Furthermore, in vivo studies were conducted to evaluate allergic responses to antigenic stimuli in beige mice.

2. Materials and methods

2.1. Animals

C57BL/6-+/+ and C57BL/6-*bg/bg* mice were purchased from Japan SLC, Inc. (Hamamatsu, Japan), and each strain was maintained by mating between the same strains. Heterozygous C57BL/6-*bg/+* mice were obtained by mating male *bg/bg* mice with female +/+ mice. Male mice aged between 10 and 16 weeks were used for all experiments. The animals were housed at a constant temperature of 22 ± 2 °C, humidity of 55 ± 10%, and an automatically controlled 12:12 h light-dark cycle, with lights on at 7:00 A.M. Food and water were provided ad libitum. This study was performed in accordance with the National Institutes of Health guidelines for the use of experimental animals. The experimental protocols were in accordance with the guidelines of the Animal Care Committee of Ehime University and approved by the University Committee for Animal Research.

2.2. Sequence analysis of the LYST mutation

Genomic DNA was isolated from tail snips of the three strains of mice using the DNeasy Tissue Kit (Qiagen, Hilden, Germany). Genomic primers flanking the murine *LYST* exon 54 (Chromosome 13-NC_000079.6) were the P3 pair, which are listed in Table 1. cDNA was synthesized from 1 μg of RNA using Avian Myeloblastosis Virus (AMV) reverse transcriptase XL and the Takara RNA PCR kit Ver. 3.0 (Takara Bio, Shiga, Japan) according to the manufacturer's instructions. Specific oligonucleotide primers (P1(+) pair and P2(−) pair) were designed to sequence exon 54 according to published sequences (NM_010748.2), as shown in Table 1. The fragment length derived from the heterozygote (*bg/+*) mice was compared with fragments generated on the reverse transcriptase reaction from the homozygote (*bg/bg*) mice and wild-type (+/+) mice using 3% agarose gel electrophoresis. PCR products were analysed, and DNA sequence traces visualized with Applied Biosystems Sequencing Analysis software (Applied Biosystems, Tokyo, Japan).

2.3. Preparation of murine peritoneal mast cells

According to the previously described method [22], PMCs were isolated by injection of HEPES-buffered Tyrode's solution (pH 7.4) into the peritoneal cavity, and the abdomen was gently massaged for 90 s. Subsequently, the peritoneal cavity was opened, and mast cell-containing fluid was collected. The collected fluid was centrifuged at 450 ×*g* for 5 min at room temperature, and the cell pellet was then resuspended in 2 ml PIPES buffer (pH 7.2) containing 119 mM NaCl, 5 mM KCl, 25 mM PIPES, 5.6 mM glucose, 0.4 mM $MgCl_2$, 1 mM $CaCl_2$, and 0.1% BSA. PMCs were separated from other cell types by layering on 3 ml of 60% percoll, and centrifuging at 450 ×*g* for 15 min at 4 °C. After the upper layer containing other components was aspirated and discarded, the remaining cell pellet of mast cells was washed with 2 ml PIPES buffer.

Table 1
The primers for gene sequencing.

Name		Sequence (5′ to 3′)
P1(+)	Forward	TGTCATCACAGCCTATACCAAC
	Reverse	CAGGAGAATGTCAGGCTTATGATG
P2(−)	Forward	TTTCCCAAATCAAATAAGCCCATA
	Reverse	GACTTTAATTGGCTAGTGTGTGCA
P3	Forward	TCCCTTCCACCTACAATGC
	Reverse	AGCTGAGTTAAGGGTGACTGC

2.4. Preparation of bone marrow-derived mast cells

BMMCs were collected from the femur and tibia and differentiated according to the method reported previously [23]. In brief, BMMCs were cultured in RPMI1640 medium containing 15% foetal calf serum, 50 U/ml penicillin, 50 μg/ml streptomycin, and 5 ng/ml IL-3 for 4 weeks and both IL-3 and 10 ng/ml stem cell factor (SCF) for a further 2 weeks in six-well plates.

BMMC maturation was verified by staining with safranin O, and expression of the FcεRI receptor and c-*kit* receptor was confirmed by flow cytometry. After the recovered cells were washed with PIPES buffer, they were attached to glass slides by a cytospin. The specimens were stained by safranin O after fixing in Carnoy's solution for 30 min and observed under a light microscope (BZ-9000, KEYENCE, Osaka, Japan). For blocking of Fc receptors in flow cytometric analysis, the cells were incubated with an anti-mouse CD32 antibody (eBioscience) at 1.0 μg per 10^6 cells in 100 μl volume for 5–10 min on ice prior to immunostaining. After washing, the cells were incubated with FITC-labelled anti-mouse FcεRI receptor antibody (1:100), PE- labelled anti-mouse c-*kit* receptor antibody (1:100), or their respective isotype-matched control antibodies (all from eBioscience) for 1 h at room temperature. The cells were analysed by a BD FACS Calibur flow cytometer and CellQuest software (BD Biosciences, NJ, USA), collecting 10,000 cells per sample.

2.5. Histological analysis of ear tissues by light microscopy and electron microscopy

For light microscope observations, ear skin tissues were rapidly removed from the mice and cut into 1 cm slices. The specimens were rinsed for 48 h with 4% paraformaldehyde in 0.1 M phosphate buffer (pH 7.4) at 4 °C and embedded in paraffin. Serial 4-μm sections were prepared, and some sections were stained with toluidine blue to highlight mast cells. Ear skin mast cells were counted individually in each section.

For visualization under a transmission electron microscope (TEM), ear skin tissues were immersed in 2.5% glutaraldehyde in PBS overnight at 4 °C, washed in 0.1 M cacodylate buffer, fixed in 1.5% osmium tetroxide for 2 h at 4 °C and then dehydrated in graded ethanol solutions. Ultrathin sections were embedded in epoxy resin and stained with uranyl acetate and lead citrate. Mast cells in the ear skin were analysed under a JEM 1230 transmission electron microscope (JEOL Ltd., Tokyo, Japan).

For scanning electron microscopic (SEM) observations, PMCs and BMMCs were attached to poly-L-Lysine-coated slides and rinsed for 24 h with 2% glutaraldehyde in 0.1 M phosphate buffer (pH 7.4) at 4 °C. Samples were rinsed with 0.1 M PBS (pH 7.4) and stained with 1% osmium tetroxide and 2% tannic acid (OTO processing). After freeze-drying with *t*-butyl alcohol, samples were coated with platinum and observed under a S-800 scanning electron microscope (Hitachi High-Technologies, Tokyo, Japan).

2.6. Fluorescence microscopy imaging of FFN206

BMMCs from the three mouse strains were harvested six weeks after cultivation, washed with PIPES buffer, and incubated with 5 μM FFN 206 (Abcam Biochemicals, Cambridge, UK) for 90 min [24]. Analysis

with confocal microscopy was performed with a Nikon A1 equipped with a filter cube (Ex = 405 nm, Em = 425–475 nm). The images were processed with NIS-Elements Advanced Research (Nikon, Tokyo, Japan).

2.7. Measurement of histamine content in skin tissues, PMCs and BMMCs

For measurement of histamine content, ear skin tissues were quickly removed, weighed and homogenized in 1 ml of 2.5% perchloric acid containing 5 mM Na_2EDTA with a Polytron homogenizer (Kinematica, Luzern, Switzerland). The homogenate was centrifuged at 10,000 ×*g* for 15 min at 4 °C, and 300 μl of supernatant was obtained. After adding 30 μl of 2 M KOH/1 M KH_2PO_4, the mixture was centrifuged at 10,000 ×*g* for 5 min at 4 °C, and the histamine concentration of the supernatant was determined using high performance liquid chromatography (HPLC)-fluorometry detection, as described previously [25]. PMCs and BMMCs in 0.5 ml of PIPES buffer were sonicated, and 20 μl of 60% perchloric acid was added. After centrifugation at 10,000 ×*g* for 5 min at 4 °C, the supernatant was applied to HPLC for histamine measurement.

2.8. Histamine release in BMMCs and PMCs

BMMCs were sensitized with 0.5 μg/ml of mouse monoclonal IgE against dinitrophenyl (DNP)-BSA for 24 h, washed twice with PIPES buffer (0.1% BSA, pH 7.2) and preincubated in PIPES buffer at 37 °C for 10 min. BMMCs and PMCs were stimulated with the indicated concentrations of DNP-BSA antigen or compound 48/80, respectively, for 30 min. These cells were also stimulated with thapsigargin, a sarcoendoplasmic reticulum Ca^{2+} ATPase inhibitor (0.5 μM), or ionomycin, a Ca^{2+} ionophore (1 μM), for 30 min. Histamine released into the medium was measured by HPLC-fluorometry [25]. Net release of histamine from cells was calculated according to the following equation:

$$\text{Net release}(\%) = (\text{responsively released histamine} - \text{non-responsively leaked histamine}) / (\text{total histamine} - \text{non-responsively leaked histamine}) \times 100.$$

$$\text{Spontaneous release}(\%) = \text{leaked histamine}/\text{total histamine} \times 100.$$

2.9. Vascular permeability and histidine decarboxylase activity after passive cutaneous anaphylaxis reaction

Passive cutaneous anaphylaxis (PCA) reactions were performed according to the previously reported method [26]. Mice were sensitized by intradermal injections of 0.5 μg/ml mouse monoclonal anti-DNP BSA IgE in one ear pinnae and 50 μl of saline in the other pinnae. After 24 h, the tail vein was injected with 0.25 ml of a mixture of 0.5% Evans blue and 1 mg/ml DNP-BSA solution. At 30 min post-injection, the mice were sacrificed under ether anaesthesia, and the ear pinnae were removed for measurement of Evans blue extravasation. Evans blue dye was extracted by incubating the ear pinnae in 0.5 ml of dimethyl sulfoxide for 24 h at 37 °C, and leakage of Evans blue was calculated by spectrometry at 650 nm.

The activity of histidine decarboxylase (HDC: a histamine synthesizing enzyme) in ear pinnae was measured 4 h post-antigen injection, as reported previously [27]. In brief, the tissues were homogenized in cold HDC solution containing 0.1 M potassium phosphate buffer, pH 6.9, 0.2 mM dithiothreitol, 0.01 mM pyridoxal 5′-phosphate, 1% (w/v) polyethylene glycol (average MW 300) and 100 μg/ml of phenylmethylsulfonyl-fluoride in a polytron and centrifuged at 10,000 ×*g* for 20 min. The clear supernatant was dialysed three times against fifty volumes of HDC buffer at 4 °C. HDC enzyme was incubated with 0.25 mM L-histidine for 4 h at 37 °C, and histamine generation was measured by HPLC-fluorometry.

2.10. Image analysis of granule area and volume

Quantitative image analyses of skin mast cells and BMMCs were performed using TEM images and confocal images, respectively. Skin mast cells were imaged by a JEM 1230 (JEOL Ltd., Tokyo, Japan). The granule area, nuclear area and cell area were measured using ImageJ software, and the area ratio of granules was calculated according to the following equation: Area ratio of granules (%) = the area of granules / (cell area − nuclear area) × 100. Z-stack images of FFN 206-loaded granules in BMMCs were imaged by confocal microscopy with a Nikon A1 (Nikon, Tokyo, Japan). The granule area, labelled by FFN206, was detected by threshold of fluorescent intensity (5–255 grey levels) with 8-bit two-dimensional images. In addition, three-dimensional images were constructed from the z-stack two-dimensional images, and the volume of FFN206-labelled granules was measured using ImageJ software.

2.11. Statistical analysis

The results are expressed as the means ± SEM. The level of statistical significance was determined using ANOVA followed by the Bonferroni multiple comparisons test. The statistical significance of differences between two groups was evaluated by Student's *t*-test. *P*-values < 0.05 were considered to indicate significant differences between groups.

3. Results

3.1. Sequence analysis of LYST genes

Because the *LYST* gene is relatively large, encoding 55 exons and spanning 207 kb, analysis was initiated at a deletion region of *LYST* gene of genomic DNA that arose at the Jackson Laboratory. A single event was identified, in which a 3-bp deletion in exon 54 resulted in the causative mutation (Fig. 1A). The deletion was predicted to influence the WD40 domain of LYST protein, which frequently acts as a stable scaffold for mediating protein-protein interactions [28]. A single band of 536-bp was indicative of a wild-type mouse, whereas a single band of 425-bp was indicative of a homozygous mouse. Two fragments were observed in all five heterozygous mice (Fig. 1B). Sequencing of the two amplified fragments revealed 3-bp deletions in exon 54 of the deletion allele (Fig. 1A).

3.2. Number of mast cells and histamine content in skin tissues

Mast cells from *bg/bg* mice had enlarged granules under light microscopy observation. Although *bg/+* mice mast cells appeared similar to +/+ mice mast cells with respect to granule size, the morphology was not clear (Fig. 2A). Transmission electron microscope observations demonstrated that *bg/+* mice mast cells had a similar granule size and shape to those of the +/+ mice mast cells, whereas the granule size of *bg/bg* mice mast cells was 1.87- and 1.76-fold larger than those of +/+ and *bg/+* mice, respectively (Fig. 2B, Table 2).

There were no significant differences in the number of mast cells in ear skin among +/+ (200.3 ± 12.2 cells/section), *bg/+* (193 ± 11.6 cells/section) and *bg/bg* (191.3 ± 10.3 cells/section) mice. Histamine content in the ear skin and PMCs of *bg/bg* mice were 57.7% and 64.8% of those of +/+ mice, respectively. There was no significant difference in the histamine content of skin tissues and PMCs between +/+ and *bg/+* mice (Table 3).

3.3. Morphological and functional analysis of BMMCs

BMMCs were cultured in the presence of IL-3 and SCF to stimulate development into the connective tissue type of mast cells [29]. Using safranin O solution, BMMC granules from *bg/bg* mice were enlarged in

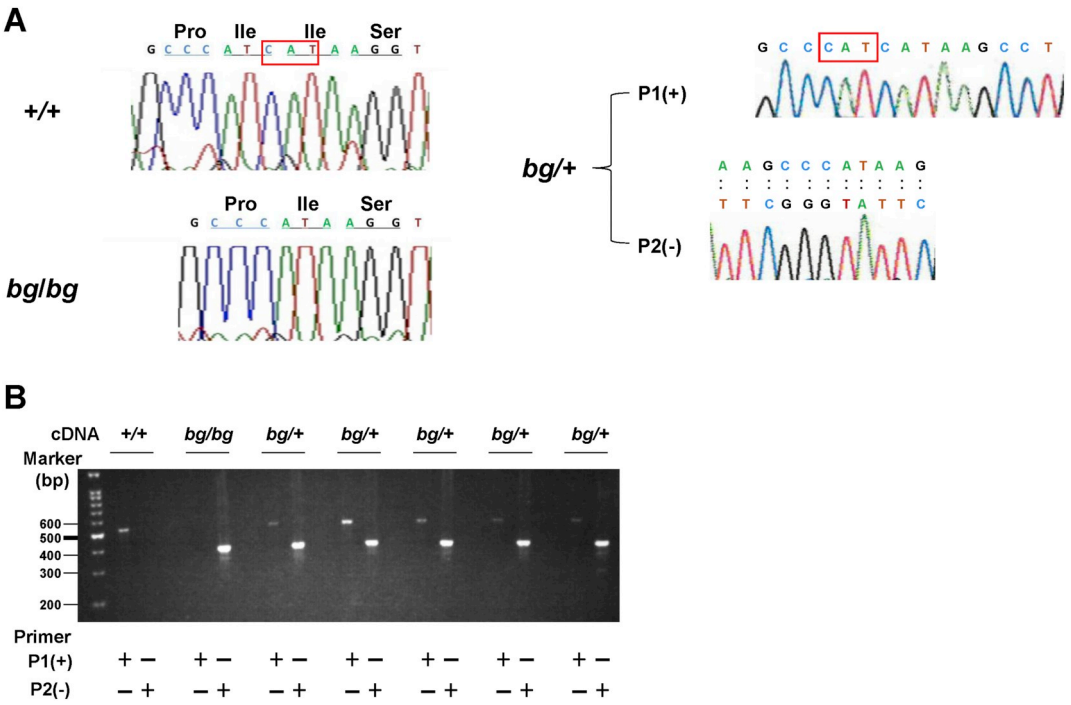

Fig. 1. Sequence analysis of genomic DNA from wild-type C57BL/6-+/+, *bg*/+ and *bg/bg* mice. The genomic primers flanking murine *LYST* exon 54 (Chromosome 13-NC_000079.6) are the P3 pair, which are listed in Table 1. The 3-bp deletion in exon 54 resulted in the causative mutation (A). Two fragments were observed in all five heterozygous mice (B).

size (Fig. 3A). From the flow cytometry analysis, the number of FcεRI+ c-*kit*+ cells was not significantly different among +/+ (94.35 ± 0.41%), *bg*/+ (97.10 ± 0.51%) or *bg/bg* (95.55 ± 0.56%) mice (Fig. 3B and C). Histamine concentrations in cell suspension medium from each of the three mouse strains began to increase from day 7 of culture, plateauing on day 21 and declining by day 28. During the entire cell culture period, histamine concentrations in BMMC suspension medium were significantly lower in *bg/bg* mice compared with *bg*/+ and +/+ mice (Fig. 3D).

Labelling with FFN206, a new fluorescent substrate of vesicular monoamine transporter 2 (VMAT2), revealed differences in the size, number and distribution of secretory granules among BMMCs derived from each mouse strain. Larger size but fewer granules were observed in *bg/bg* BMMCs compared with those from *bg*/+ and +/+ mice (Fig. 4). The size and number of granules in *bg*/+ and +/+ BMMCs were almost identical, and small granules were widely distributed throughout the whole cell plasma membrane, as evidenced by three-dimensional structured photos.

3.4. Morphological changes in PMCs and BMMCs after degranulation by scanning electron microscopy

Scanning electron microscopic examination showed ridge-like folds of plasma membrane extending from the cell surface of PMCs from each of the three mouse strains. When exocytotic degranulation was triggered by compound 48/80 stimulation, numerous spherical granules were secreted and attached to the cell surface of *bg*/+ and +/+ PMCs, whereas enlarged size but fewer granules were observed in *bg/bg* mice PMCs (Fig. 5A). The ridge-like folds were also observed in *bg/bg*, *bg*/+ and +/+ BMMCs without stimulation. The addition of 10 μg/ml compound 48/80 caused the secretion of spherical granules, as shown in PMCs (Fig. 5B).

3.5. Histamine release responses in PMCs and BMMCs after stimulation with several secretagogues

After the addition of compound 48/80, histamine release was observed by PMCs from all three mouse strains at the lowest concentration (1 μg/ml) and increased in a dose-dependent manner (Fig. 6A). The efficacy of responses was higher in *bg/bg* mice than *bg*/+ and +/+ mice. In *bg/bg* mice PMCs, histamine release in response to 0.5 μM thapsigargin was 1.21- and 1.25-fold higher than that of *bg*/+ and +/+ mice, respectively. In response to 1 μM ionomycin, histamine release from PMCs of *bg/bg* mice was 1.21- and 1.59-fold greater than that of *bg*/+ and +/+ mice, respectively (Fig. 6B).

After the addition of DNP-BSA, histamine release from BMMCs from all three mouse strains occurred at the lowest concentration (2 ng/ml DNP-BSA) and increased in a dose-dependent manner (Fig. 6C). The histamine release response pattern in *bg/bg* BMMCs also showed higher efficacy than *bg*/+ and +/+ mice.

Histamine release occurred in BMMCs from all three mouse strains in response to 10 μg/ml of compound 48/80, and the histamine release response in *bg/bg* mice BMMCs was 1.26- and 1.31-fold higher than that of *bg*/+ and +/+ mice, respectively (Fig. 6D).

Histamine release responses of *bg/bg* BMMCs were 1.70- (0.5 μM thapsigargin) and 1.64-fold (1 μM ionomycin) higher than those of *bg*/+ mice BMMCs, and 1.65- (0.5 μM thapsigargin) and 1.61-fold (1 μM ionomycin) higher than those of +/+ mice BMMCs (Fig. 6D).

The release patterns of β-hexosaminidase, another exocytotic component, in granules from PMCs and BMMCs were similar to those of histamine release and were also the highest in *bg/bg* mice compared with *bg*/+ and +/+ mice (data not shown).

3.6. Passive cutaneous anaphylaxis (PCA) reaction in vivo

In the ear pinnae tissues that were sensitized by monoclonal IgE against DNP-BSA, the extravasation of Evans blue dye was determined 30 min after DNP-BSA antigen stimulation. There was no significant difference in the increasing rate of dye leakage of the IgE-sensitized site

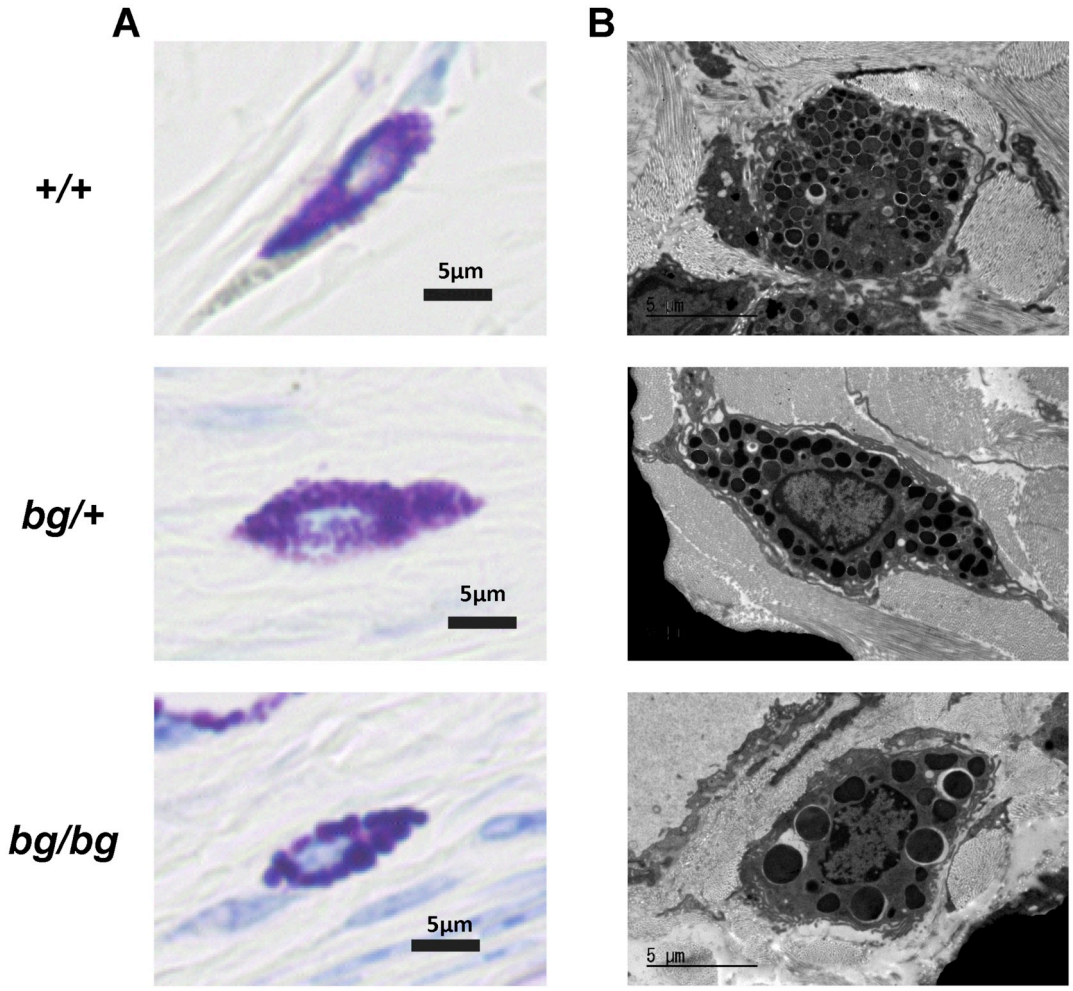

Fig. 2. Histological analysis of CTMCs in ear skin tissues.
Light micrographs of mast cells detected by toluidine blue staining in ear skin tissues of +/+, *bg/+* and *bg/bg* mice (A). Transmission electron micrographs of mast cells detected in ear skin tissues of +/+, *bg/+* and *bg/bg* mice (B).

Table 2
Granule size in mast cells from ear skin.

	+/+	*bg/+*	*bg/bg*
Maximum diameter (μm)	0.92 ± 0.03	0.98 ± 0.06	1.72 ± 0.14**,††

The three largest granules in each five mast cells of ear skin from the three different strains were analysed by TEM, and the maximum diameter was measured. The data are shown as the means ± S.E.M. (n = 15).
** $P < 0.01$ vs. +/+.
†† $P < 0.01$ vs. *bg/+* mice.

Table 3
Histamine contents in skin tissues and peritoneal mast cells.

	+/+	*bg/+*	*bg/bg*
Ear skin (nmol/g) (n = 4)	1097.61 ± 52.39	1091.50 ± 58.57	632.92 ± 100.74**,††
Peritoneal mast cells (pmol/10^4 cells) (n = 3)	492.51 ± 16.98	475.30 ± 9.11	318.96 ± 12.32**,††

The data are shown as the means ± S.E.M.
** $P < 0.01$ vs. +/+.
†† $P < 0.01$ vs. *bg/+* mice.

to the saline injected site among *bg/bg*, *bg/+*, and +/+ mice (Table 4). Histamine contents of IgE-treated ear pinnae were decreased compared with saline-treated ear pinnae 4 h after DNP-BSA stimulation, at 30.4% and 41.7% in *bg/bg* and +/+ mice, respectively (Fig. 7A). An increase in HDC activity was observed in IgE-treated ear pinnae compared with saline controls (2.07-fold and 1.92-fold in *bg/bg* and +/+ mice, respectively), but the increased ratio was not different between these two strains (Fig. 7B).

3.7. Image analysis of granule area and volume in skin MCs and BMMCs

Image analyses were performed to compare the volume of granules in PMCs and BMMCs between +/+ and *bg/bg* mice. The area ratios of granules to cytosol in +/+ and *bg/bg* skin mast cells using TEM images were 49.6 ± 1.19% (n = 3) and 32.32 ± 4.83% (n = 4), respectively, that is, the total area of vesicles in *bg/bg* mice was 65.2% that of +/+ mice (Fig. 8A). Since this ratio was calculated from two-dimensional electron microscopy photos, the volume ratio after calculation from two-dimensions to three-dimensions was 53% which is similar to the ratio of histamine content. An FFN fluorescent probe was trapped into the vesicle, and each two-dimensional image was obtained at the equal 1 μm z-stack intervals by confocal microscopy (Fig. 8B). The sum of the vesicle area in each image was assumed to be the volume of vesicles in a cell. The relative volume rates of granules to the whole cell in +/+ and *bg/bg* BMMCs were 100.0 ± 39.14% (n = 3) and 28.02 ± 3.07% (n = 4), respectively, showing that the total volume of *bg/bg* mice was

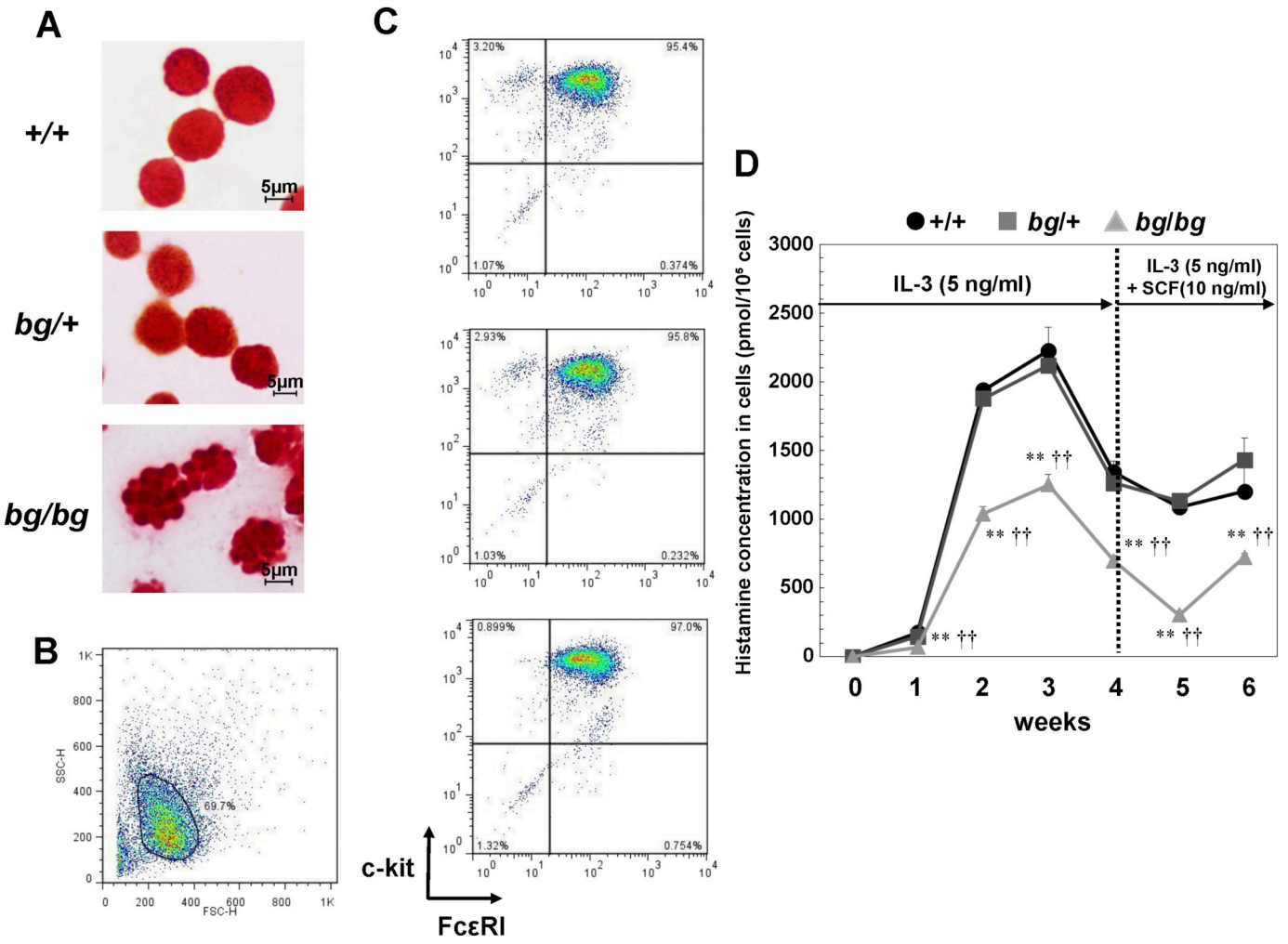

Fig. 3. Maturation of 6-week BMMC cultures and changes in histamine contents in cell suspension during differentiation
BMMCs from +/+, *bg*/+ and *bg/bg* mice were stained with safranin O after 6 weeks of culture and observed by light microscopy (A). The expression of FcεRI receptor and c-*kit* receptor in BMMCs were analysed using a BD FACS Calibur flow cytometer. The gating information (B) and representative plots (C) of FcεRI receptor and c-*kit* receptor expression in total BMMCs are shown. The data are from one of at least 3 separate experiments with similar results (FL1-H: FcεRI, FL2-H: c-*kit*). Histamine contents in BMMCs of +/+ (●), *bg*/+ (■), and *bg/bg* (▲) mice were measured every 7 days after the start of culture (D). The histamine content is expressed as pmol/10^5 cells. $^{**}P < 0.01$ vs. +/+ mice, $^{\dagger\dagger}P < 0.01$ vs. *bg*/+ mice. Each point represents the mean ± S.E.M. of three groups for 1–2 weeks and five groups for 3–6 weeks.

28.02% that of +/+ mice. These were rough calculations because of the limited number of images from one cell, and each vesicle volume was calculated as a column instead of a sphere.

4. Discussion

CHS is a rare recessive disease characterized by hypopigmentation, recurrent infection, mild coagulation defects and neurological problems. Beige mice display the above symptoms and are considered to be an appropriate animal model of human CHS. The absence of CHS/LYST protein results in enlarged mast cell granules, and many studies have been performed to clarify the degranulation processes, both morphologically and with electrophysiological techniques. Mast cells play important roles in allergy, but few reports have been published on mast cell function and its relation to histamine effects in CHS. Therefore, we sought to confirm the mutation of the *LYST* gene in homozygote and heterozygote beige strains accompanied by morphological and functional studies of mast cells.

This study confirmed the presence of a 3-bp deletion in exon 54 of the *LYST* gene encoding the WD region of *bg/bg* mice, as previously reported. Two fragments of genomic DNA of exon 54 of the *LYST* gene derived from +/+ and *bg/bg* mice were observed in *bg*/+ mice. Since the *LYST* mutation showed an autosomal recessive inheritance pattern [30], the characteristics of *bg*/+ mice mast cells should be the same as those of +/+ mice mast cells. Indeed, the size of histamine granules, histamine content and the exocytotic responses to stimulants in *bg*/+ mice mast cells were almost identical to those of +/+ mast cells. In contrast, *bg/bg* mice mast cells showed larger sized granules, lower histamine content and an increased histamine release ratio than +/+ and *bg*/+/+ mice.

Bone marrow cells can differentiate into two types of mast cells, mucosal mast cells (MMCs) and connective tissue-type mast cells (CTMCs). In this study, BMMCs cultured in the presence of only IL-3 for the first 4 weeks and a combination of IL-3 and stem cell factor for the subsequent two weeks differentiated into CTMCs that were confirmed morphologically by safranin O staining and pharmacologically with response to compound 48/80 stimulation. The mechanism of the CTMC response to cationic substances, such as compound 48/80 and cationic peptides, has remained contradictory, but Mas-related G protein coupled receptor (Mrgpr) B2 was identified as a receptor for these ligands [31].

BMMCs of *bg/bg* mice also showed characteristics of CTMCs, such as

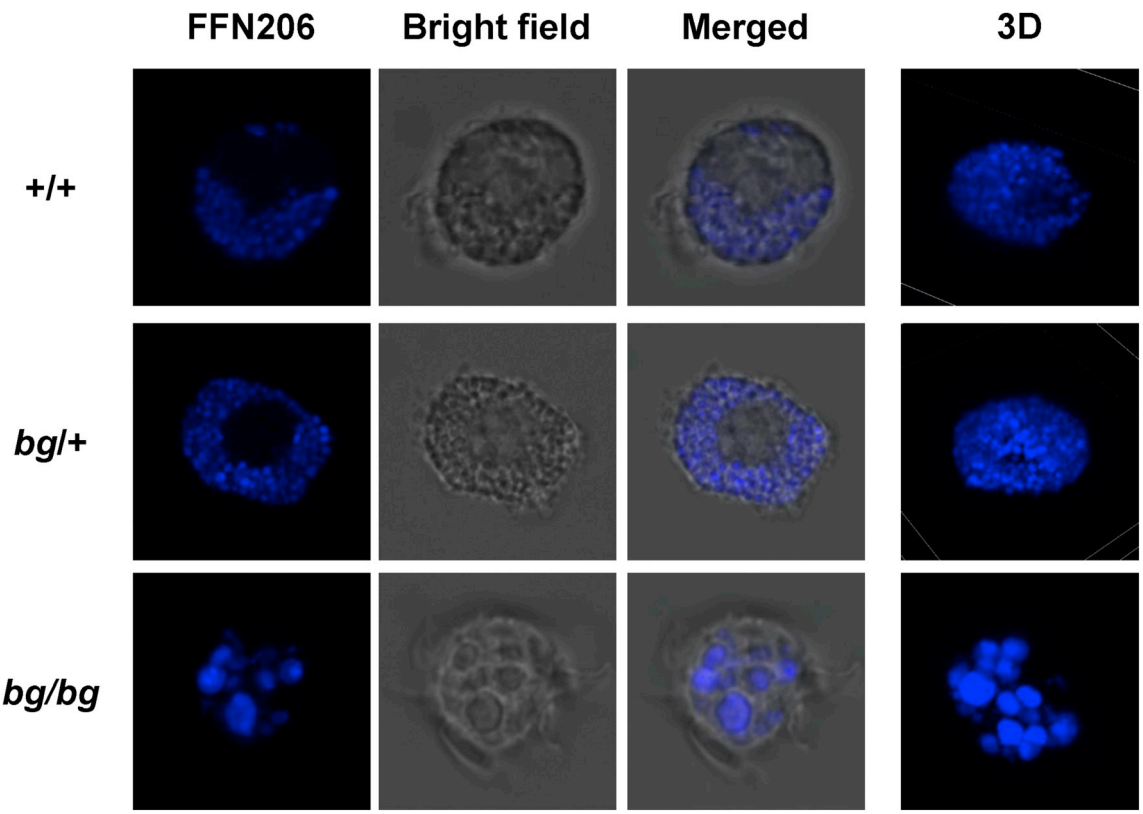

Fig. 4. Confocal fluorescence images of BMMCs labelled with FFN206
BMMCs of +/+, *bg/+* and *bg/bg* mice were loaded with 5 μM of FFN206, washed and imaged by confocal microscopy. Fluorescence images (Ex = 405 nm, Em = 425–475 nm), Bright field image merged with fluorescence and bright field images. Three-dimensional images were constructed using the NIS-Elements Advanced Research software (Nikon).

the response to compound 48/80. When BMMCs were cultured with only IL-3, BMMCs differentiated into MMCs. The numbers of FcεRI+ and Kit+ cells were 35.14%, 53.14% and 51.13% in *bg/bg*, *bg/+*, and +/+ mice, respectively, and delayed differentiation was observed in *bg/bg* mice mast cells compared to +/+ and *bg/+* mast cells in our previous report [32]. The addition of stem cell factor resulted in complete differentiation, showing 94–97% FcεRI+ and Kit+ cells in the cultures of these strains. In this study, there were no differences in the number of connective tissue mast cells in ear skin among the three different strains (*bg/bg*, *bg/+* and +/+). It is possible that SCF

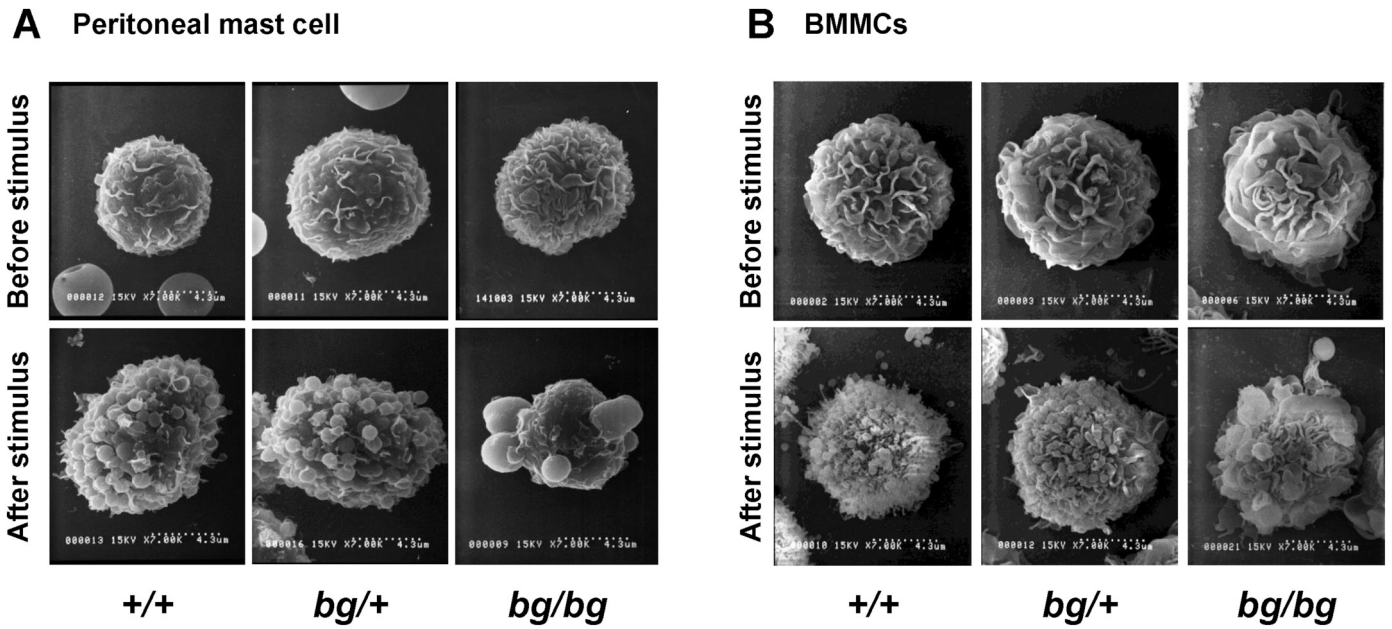

Fig. 5. Morphological changes of PMCs and BMMCs after degranulation by SEM.
PMCs (A) and BMMCs (B) from +/+, *bg/+* and *bg/bg* mice were stimulated with 10 μg/ml compound 48/80 for 30 min and observed by SEM (5000×).

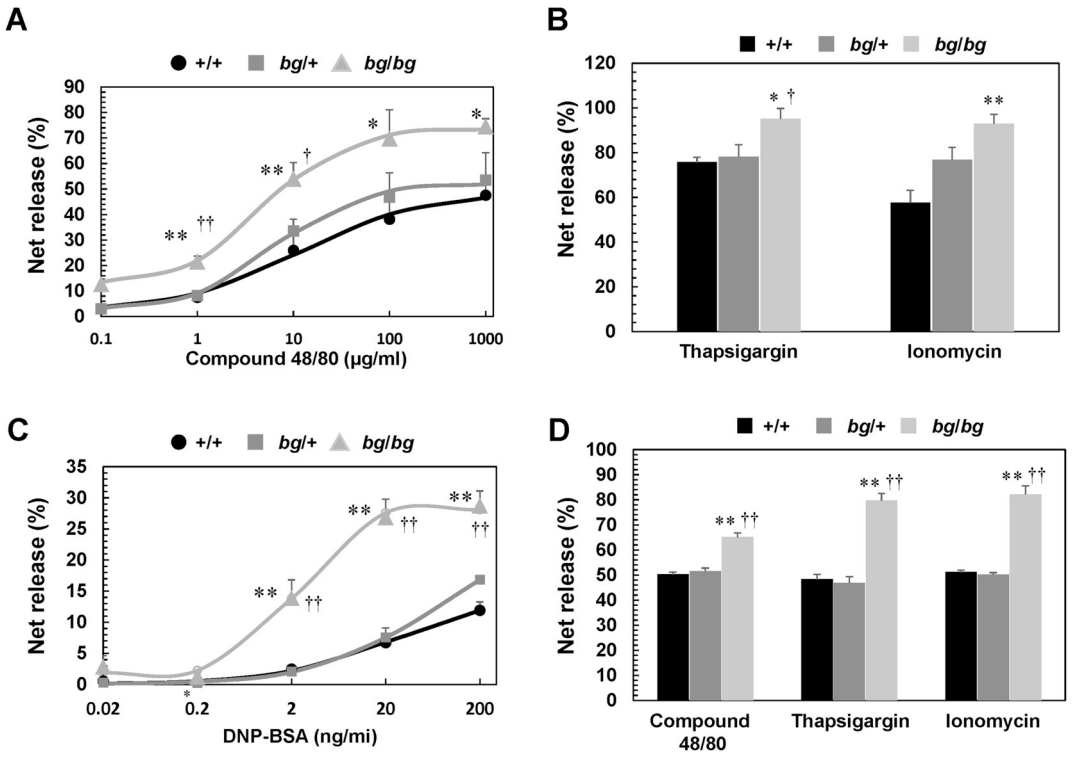

Fig. 6. Net histamine release of PMCs and BMMCs of +/+, *bg*/+ and *bg/bg* mice stimulated by several secretagogues
Peritoneal mast cells of +/+ *bg*/+ and *bg/bg* mice were stimulated with different concentrations of compound 48/80 (0.1, 1, 10, 100 μg/ml and 1 mg/ml) for 30 min (A) or thapsigargin (0.5 μM) and ionomycin (1 μM) for 30 min (B). The spontaneous release of +/+, *bg*/+ and *bg/bg* PMCs was 3.48 ± 0.43%, 4.32 ± 0.30% and 16.20 ± 1.07%, respectively. BMMCs of +/+ *bg*/+ and *bg/bg* mice were sensitized with 0.5 μg/ml of anti DNP-BSA monoclonal IgE overnight and stimulated with DNP-BSA antigen (0.02, 0.2, 2, 20, 200 ng/ml) for 30 min (C) and compound 48/80 (10 μg/ml), thapsigargin (0.5 μM) and ionomycin (1 μM) (D). The spontaneous release of +/+, *bg*/+ and *bg/bg* BMMCs was 0.45 ± 0.18%, 0.37 ± 0.13% and 1.55 ± 0.34%, respectively. $^{*}P < 0.05$, $^{**}P < 0.01$ vs. +/+ mice. $^{\dagger}P < 0.05$, $^{\dagger\dagger}P < 0.01$ vs. *bg*/+ mice. Each point represents the mean ± S.E.M. of five groups for (A), three groups for (B), six groups for (C) and three groups for (D).

Table 4
Increased ratio of Evans blue dye extravasation after passive cutaneous anaphylaxis reaction.

Mice strain	Fold
+/+	2.05 ± 0.27
bg/+	1.97 ± 0.32
bg/bg	2.14 ± 0.30

Data are means ± S.E.M. (n = 4).
Extravasation of Evans blue dye revealed increased permeability, expressed as the ratio of quantity of Evans blue dye in the ear skin sensitized with IgE to that of the non-sensitized ear skin (control group).

stimulation promotes differentiation that is affected by the *LYST* mutation.

A new fluorescent probe, FFN206, was recently introduced and is highly sensitive to VMAT2 [24]. This compound is capable of detecting VMAT2 activity in intact cells using fluorescence microscopy, with subcellular localization to VMAT2-expressing acidic compartments without apparent labelling of other organelles. Because histamine synthesized in the cytosol is transported into secretory granules via VMAT2 and stored in mast cells, FFN206 is easily trapped in granules, making it a good tool for labeling granules. In this research, we demonstrated the labelling of secretory granules of living mast cells with an FFN206 probe using three-dimensional confocal microscopy [32]. FFN206 selectively labels mast cell granules, demonstrating the large size yet low number of granules in *bg/bg* mast cells and the small size yet high number of granules in *bg*/+ and +/+ mice (Fig. 4). FFN206 is therefore a useful tool for analysing the process of granule fusion in mast cells.

The ratio of histamine release from PMCs was higher in *bg/bg* mice relative to those of *bg*/+ and +/+ mice after stimulation with 48/80. Additionally, the ratio of histamine release from BMMCs was also higher in *bg/bg* mice compared with *bg*/+ and +/+ mice after stimulation with compound 48/80 and DNP-BSA antigen. These results are similar to findings in beige rat PMCs [21]. This enhancement of histamine release may relate to exocytotic events because the lifetime of the fusion pore of PMCs is 0.058 s in +/+ mice, whereas it is substantially longer at 0.36 s in *bg/bg* mice, according to capacitance measurements [33].

In the PCA reaction, marked histamine release occurred, and the remaining histamine content in the ear skin of *bg/bg* and +/+ mice was 30.4% and 41.7%, respectively, demonstrating enhanced in vivo histamine release in *bg/bg* mice compared with +/+ mice. There was no significant difference in the extravasation of Evans blue dye in PCA reactions among *bg/bg*, *bg*/+ and +/+ mice. Because dye leakage caused by increased cell permeability is dependent on the early phase of the reaction induced by histamine, the lower content but higher release ratio of histamine in *bg/bg* mice may lead to the same PCA response as that in +/+ mice. In the mucosal mast cell line, rat basophilic leukaemia (RBL)-2H3 cells, IgE-mediated stimulation caused increased activity of histidine decarboxylase (HDC), a histamine synthesizing enzyme for 2 to 4 h, suggesting that IgE-mediated cell signalling, such as increases in intracellular Ca^{2+} concentrations and the activation of protein kinase C (PKC), may have induced HDC activation [27]. In the present study, increased activity of HDC in PCA reactions was observed in both *bg/bg* and +/+ mice skin. It was reported that painting phorbol myristate acetate (PMA) on mouse skin resulted in a marked increase of HDC activity in the dermis, and this increase was attributed to the

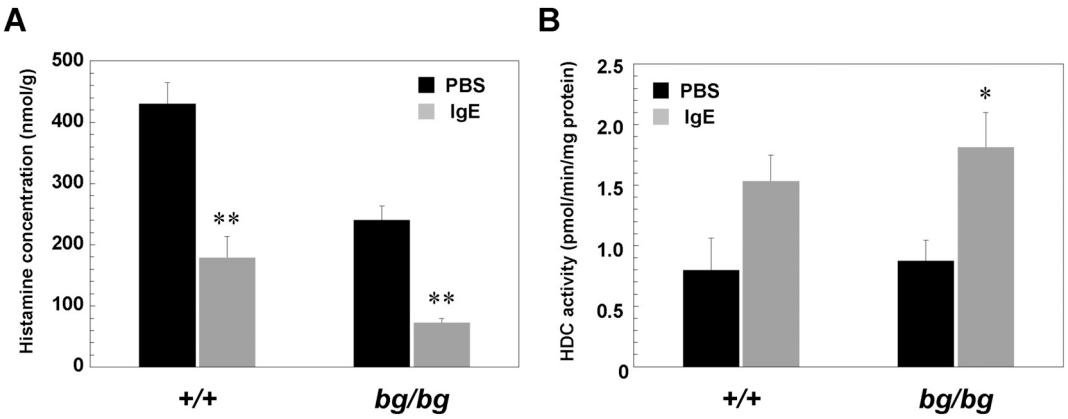

Fig. 7. Passive cutaneous anaphylaxis reaction in the ear skins of +/+ and *bg/bg* mice.
The passive cutaneous anaphylaxis reactions in the ear skins of +/+ and *bg/bg* mice are shown. In the right side of the mouse ear, 50 µl of mouse anti-DNP-BSA monoclonal IgE (0.5 µg/ml) was injected subcutaneously, and 0.25 ml of the mixture of 1 mg DNP-BSA and 1% Evans blue was injected into the tail vein 24 h later (grey column). The same volume of PBS was injected into the left ear as a control. After 4 h, the ear skin was removed and homogenized, and histamine contents (A) and HDC activity (B) were measured according to the methods described in the Materials and methods. Black and grey columns show the control and DNP-BSA-treated group, respectively. $*P < 0.05$, $**P < 0.01$ vs. the control group (PBS treatment). Each point represents the mean ± S.E.M. from six *bg/bg* and four +/+ mice.

recruitment of leucocytes from the bone marrow [34]. In this PCA reaction, only localized mast cells were targeted for stimulation by IgE-mediated antigen. Therefore, we assumed that this increase was mainly attributed to mast cells. In this research, we could not demonstrate a difference in HDC activity between *bg/bg* and +/+ mice, suggesting that the signalling transduction resulting in HDC activation occurred normally in *bg/bg* mice.

In this experiment, the histamine concentration in skin in *bg/bg* mice was lower than that of +/+ mice, even though the mast cell number was the same between these strains. Moreover, the histamine contents of peritoneal mast cells and BMMCs of *bg/bg* mice were lower than those of +/+ mice. Although Hamel et al. demonstrated larger granules in *bg/bg* mice, the volume of which was > 18-fold that of +/+ mice mast cell secretory granules, the total volume of granules in each mast cell was the same between these strains [35]. In this research, we found a difference in the total volume of secretory granules between

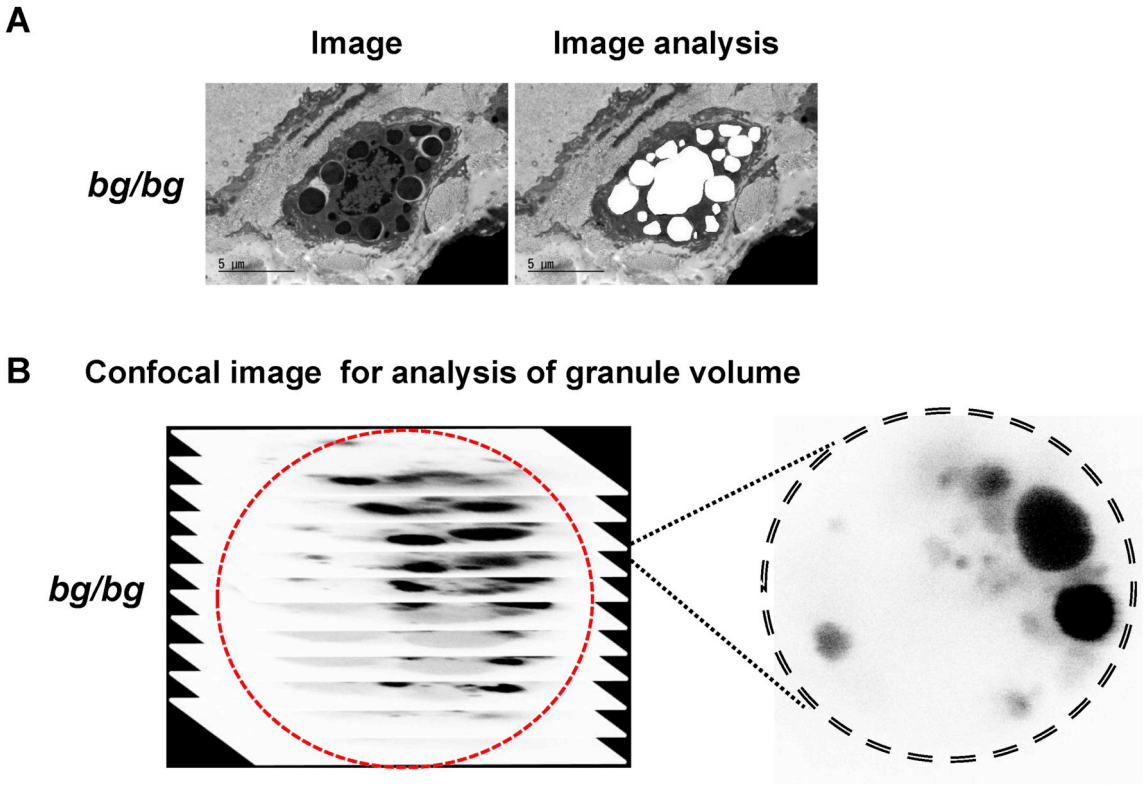

Fig. 8. Image analysis of granule area and volume in skin mast cells and BMMCs of +/+ and *bg/bg* mice.
The total area of granules was obtained by adding each granule area shown as white spots in skin mast cells using TEM images, as illustrated in the photo in Fig. 2. The area ratio of granules to cytosol was calculated according to the equation described in the Materials and methods (A). The volume of FFN-labelled granules in BMMCs was measured using Z-stack pictures at 0.5 µm intervals, as obtained by confocal microscopy. The total granule volume was obtained by the addition of granule areas, as demonstrated on each stack picture (B).

bg/bg and +/+ mice after calculation using obtained images by electron microscopy and confocal microscopy labelled with fluorescent FFN probes, which are trapped in the mast cell granules via VMAT2. The histamine content in *bg/bg* mast cells was less than that of +/+ mice in proportion to the total volume of granules in each mast cell of these strains.

Although mast cell secretory granules are regarded as lysosome-related organelles or secretory lysosomes, their molecular mechanisms of biogenesis remain uncertain. Several models of biogenesis of mast cell granules have been proposed. Hammel et al. proposed the unit addition mechanism for the synthesis of mast cell granules by analysing the volume and number of granules from electron microscopy plane images [35]. First, the smallest progranules produced at the Golgi cisterna were fused with homotypic unit granules to produce immature granules by the unit addition mechanism, of which size was multi modal, and finally changed to mature granules [36]. Large granules were observed in mast cells with the *CHS/BEACH* mutation, which was produced by random fusion of heterotypic granules. LYST is thought to interact with signalling proteins as a scaffold and negatively regulate homotypic granule fusion [37].

The GTPase Rab5 is related to endocytotic process and controls secretory granule size and cargo composition, and constitutively active Rab5 mutants induce few and enlarged secretory granules in RBL-2H3 cells [38]. The expression of constitutively active Rab5 leads to enhanced β-hexosaminidase release. Future studies should be conducted to clarify whether the activity of GTPase Rab5 is related to the *LYST* mutation.

It is well known that the pathogenesis of CHS is the result of the *LYST* gene mutation. Tchernev et al. demonstrated that LYST interacts with proteins involved in vesicular transport and signal transduction, such as 14-3-3, casein kinase II, and hepatocyte growth factor-regulated tyrosine kinase substrate (HRS), and orchestrates the degranulation machinery of tethering, docking and fusion of the vesicular and plasma membrane [6]. Recently, we found a relationship between a unique member of the Ca^{2+}-release-activated calcium (CRAC) family of Ca^{2+}-selective channels, CRACM3, and syntaxin 4 in RBL-2H3 cells. Knockdown of CRACM3 suppressed functional exocytosis by decreasing the open time of the vesicle fusion pore [39]. Prolongation of fusion pore open time in beige mast cells may be explained by the modification of CRACM3 channels through interactions between LYST and syntaxin.

In conclusion, we confirmed that beige mice mast cells have a lower histamine content and a higher rate of histamine release compared with heterozygote and wild-type mice after determining the genotype of the *LYST* mutation. Furthermore, we revealed that the morphological and functional characteristics of mast cells in heterozygote mice were similar to those of wild-type mice. Even though the pattern of mast cell responses to secretagogues in beige mice is different from those of heterozygote and wild-type mice, the PCA reactions observed in vivo were not different among these strains.

Acknowledgements

We would like to thank professor M. Yamashita (Dept. of Immunology, Pathogenesis and Pathophysiology, Ehime University Graduate School of Medicine) for the generous supply of IL-3. We also thank Assistant Professor K. Kameda and Drs. T. Tsujita, Y. Tanaka and N. Tokunaga (Division of Analytical Bio-medicine, Advanced Research support Center, Ehime university) for their technical advice and support.

Competing interests

The authors declare that they have no competing interests.

Author's contribution

KM, SL and MO conceived and designed the study. TK performed experiments, analysed the data and wrote the first daft. MNAS and MS analysed and interpreted data. MM proofread and revised the submission. All authors contributed to writing the manuscript and approved the final version of the manuscript.

Funding

M.M. was funded by the Japan Society for the Promotion of Science, KAKENHI Grant 25462220. S.L. was supported by the Japan Society for the Promotion of Science, KAKENHI Grant 15K19575.

References

[1] R.A. Spritz, Genetic defects in Chediak-Higashi syndrome and the beige mouse, J. Clin. Immunol. 18 (2) (1998) 97–105.
[2] J.I. Gallin, J.S. Bujak, E. Patten, S.M. Wolff, Granulocyte function in the Chediak-Higashi syndrome of mice, Blood 43 (2) (1974) 201–206.
[3] J. Kaplan, I. De Domenico, D.M. Ward, Chediak-Higashi syndrome, Curr. Opin. Hematol. 15 (1) (2008) 22–29.
[4] D.J. Prieur, L.L. Collier, Animal model of human disease: Chediak-Higashi syndrome, Am. J. Pathol. 90 (2) (1978) 533–536.
[5] D.L. Nagle, M.A. Karim, E.A. Woolf, L. Holmgren, P. Bork, D.J. Misumi, S.H. McGrail, B.J. Dussault Jr., C.M. Perou, R.E. Boissy, G.M. Duyk, R.A. Spritz, K.J. Moore, Identification and mutation analysis of the complete gene for Chediak-Higashi syndrome, Nat. Genet. 14 (3) (1996) 307–311.
[6] V.T. Tchernev, T.A. Mansfield, L. Giot, A.M. Kumar, K. Nandabalan, Y. Li, V.S. Mishra, J.C. Detter, J.M. Rothberg, M.R. Wallace, F.S. Southwick, S.F. Kingsmore, The Chediak-Higashi protein interacts with SNARE complex and signal transduction proteins, Mol. Med. 8 (1) (2002) 56–64.
[7] N. Durchfort, S. Verhoef, M.B. Vaughn, R. Shrestha, D. Adam, J. Kaplan, D.M. Ward, The enlarged lysosomes in beige j cells result from decreased lysosome fission and not increased lysosome fusion, Traffic 13 (1) (2012) 108–119.
[8] M. Ito, F. Tanabe, Y. Takami, A. Sato, S. Shigeta, Rapid down-regulation of protein kinase C in (Chediak-Higashi syndrome) beige mouse by phorbol ester, Biochem. Biophys. Res. Commun. 153 (2) (1988) 648–656.
[9] M. Ito, A. Sato, F. Tanabe, E. Ishida, Y. Takami, S. Shigeta, The thiol proteinase inhibitors improve the abnormal rapid down-regulation of protein kinase C and the impaired natural killer cell activity in (Chediak-Higashi syndrome) beige mouse, Biochem. Biophys. Res. Commun. 160 (2) (1989) 433–440.
[10] F. Tanabe, S.H. Cui, M. Ito, Abnormal down-regulation of PKC is responsible for giant granule formation in fibroblasts from CHS (beige) mice—a thiol proteinase inhibitor, E-64-d, prevents giant granule formation in beige fibroblasts, J. Leukoc. Biol. 67 (5) (2000) 749–755.
[11] H. Kasai, F. Tanabe, Enhanced diacylglycerol production by phospholipase D activation is responsible for abnormal increase in concanavalin a cap formation in polymorphonuclear leukocytes from Chediak-Higashi syndrome (beige) mice, Int. Immunopharmacol. 21 (1) (2014) 193–199.
[12] S.J. Galli, S. Nakae, M. Tsai, Mast cells in the development of adaptive immune responses, Nat. Immunol. 6 (2) (2005) 135–142.
[13] P.K. Crowle, D.E. Phillips, Characteristics of mast cells in Chediak-Higashi mice: light and electron microscopic studies of connective tissue and mucosal mast cells, Exp. Cell Biol. 51 (3) (1983) 130–139.
[14] E.Y. Chi, D. Lagunoff, Abnormal mast cell granules in the beige (Chediak-Higashi syndrome) mouse, J. Histochem. Cytochem. 23 (2) (1975) 117–122.
[15] E.Y. Chi, E. Ignacio, D. Lagunoff, Mast cell granule formation in the beige mouse, J. Histochem. Cytochem. 26 (2) (1978) 131–137.
[16] K.C. Poon, P.I. Liu, S.S. Spicer, Mast cell degranulation in beige mice with the Chediak-Higashi defect, Am. J. Pathol. 104 (2) (1981) 142–149.
[17] E. Crivellato, L. Candussio, G. Decorti, F.B. Klugmann, F. Mallardi, Adriamycin induces exocytosis in rat and beige mouse peritoneal mast cells: an ultrastructural, morphometric and biochemical study, J. Submicrosc. Cytol. Pathol. 31 (2) (1999) 279–286.
[18] A.M. Dvorak, I. Hammel, S.J. Galli, Beige mouse mast cells generated in vitro: ultrastructural analysis of maturation induced by sodium butyrate and of IgE-mediated, antigen-dependent degranulation, Int. Arch. Allergy Appl. Immunol. 82 (3–4) (1987) 261–268.
[19] Y. Kitamura, M. Shimada, K. Hatanaka, Y. Miyano, Development of mast cells from grafted bone marrow cells in irradiated mice, Nature 268 (5619) (1977) 442–443.
[20] K. Hatanaka, Y. Kitamura, Y. Nishimune, Local development of mast cells from bone marrow-derived precursors in the skin of mice, Blood 53 (1) (1979) 142–147.
[21] T. Jippo-Kanemoto, T. Kasugai, A. Yamatodani, H. Ushio, T. Mochizuki, K. Tohya, M. Kimura, M. Nishimura, Y. Kitamura, Supernormal histamine release and normal cytotoxic activity of beige (Chediak-Higashi syndrome) rat mast cells with giant granules, Int. Arch. Allergy Immunol. 100 (2) (1993) 99–106.
[22] N. Inagaki, N. Nakai, M. Kimata, H. Kawasaki, H. Nagai, Recovery of purification-associated reduction in antigen-induced histamine release from rat peritoneal mast cells, Biol. Pharm. Bull. 24 (7) (2001) 829–834.
[23] M. Tachibana, K. Wada, K. Katayama, Y. Kamisaki, K. Maeyama, T. Kadowaki,

R.S. Blumberg, A. Nakajima, Activation of peroxisome proliferator-activated receptor gamma suppresses mast cell maturation involved in allergic diseases, Allergy 63 (9) (2008) 1136–1147.
[24] G. Hu, A. Henke, R.J. Karpowicz Jr., M.S. Sonders, F. Farrimond, R. Edwards, D. Sulzer, D. Sames, New fluorescent substrate enables quantitative and high-throughput examination of vesicular monoamine transporter 2 (VMAT2), ACS Chem. Biol. 8 (9) (2013) 1947–1954.
[25] A. Yamatodani, H. Fukuda, H. Wada, T. Iwaeda, T. Watanabe, High-performance liquid chromatographic determination of plasma and brain histamine without previous purification of biological samples: cation-exchange chromatography coupled with post-column derivatization fluorometry, J. Chromatogr. 344 (1985) 115–123.
[26] T. Oka, J. Kalesnikoff, P. Starkl, M. Tsai, S.J. Galli, Evidence questioning cromolyn's effectiveness and selectivity as a 'mast cell stabilizer' in mice, Lab. Investig. 92 (10) (2012) 1472–1482.
[27] K. Maeyama, Y. Taguchi, M. Sasaki, H. Wada, M.A. Beaven, T. Watanabe, Induction of histidine decarboxylase of rat basophilic leukemia (2H3) cells stimulated by higher oligomeric IgE or phorbol myristate acetate, Biochem. Biophys. Res. Commun. 151 (3) (1988) 1402–1407.
[28] C.M. Trantow, M. Mao, G.E. Petersen, E.M. Alward, W.L. Alward, J.H. Fingert, M.G. Anderson, Lyst mutation in mice recapitulates iris defects of human exfoliation syndrome, Invest. Ophthalmol. Vis. Sci. 50 (3) (2009) 1205–1214.
[29] D.D. Metcalfe, Mast cells and mastocytosis, Blood 112 (4) (2008) 946–956.
[30] A.R. Cullinane, A.A. Schaffer, M. Huizing, The BEACH is hot: a LYST of emerging roles for BEACH-domain containing proteins in human disease, Traffic 14 (7) (2013) 749–766.
[31] B.D. McNeil, P. Pundir, S. Meeker, L. Han, B.J. Undem, M. Kulka, X. Dong, Identification of a mast-cell-specific receptor crucial for pseudo-allergic drug reactions, Nature 519 (7542) (2015) 237–241.
[32] T. Kiyoi, S. Liu, M.N.A. Sahid, M. Shudou, K. Maeyama, M. Mogi, High-throughput screening system for dynamic monitoring of exocytotic vesicle trafficking in mast cells, PLoS One 13 (6) (2018) e0198785.
[33] G. Alvarez de Toledo, R. Fernandez-Chacon, J.M. Fernandez, Release of secretory products during transient vesicle fusion, Nature 363 (6429) (1993) 554–558.
[34] Y. Taguchi, K. Tsuyama, T. Watanabe, H. Wada, Y. Kitamura, Increase in histidine decarboxylase activity in skin of genetically mast-cell-deficient W/Wv mice after application of phorbol 12-myristate 13-acetate: evidence for the presence of histamine-producing cells without basophilic granules, Proc. Natl. Acad. Sci. U. S. A. 79 (22) (1982) 6837–6841.
[35] I. Hammel, A.M. Dvorak, S.J. Galli, Defective cytoplasmic granule formation. I. Abnormalities affecting tissue mast cells and pancreatic acinar cells of beige mice, Lab. Investig. 56 (3) (1987) 321–328.
[36] I. Hammel, D. Lagunoff, S.J. Galli, Regulation of secretory granule size by the precise generation and fusion of unit granules, J. Cell. Mol. Med. 14 (7) (2010) 1904–1916.
[37] N.P. Azouz, I. Hammel, R. Sagi-Eisenberg, Characterization of mast cell secretory granules and their cell biology, DNA Cell Biol. 33 (10) (2014) 647–651.
[38] N.P. Azouz, N. Zur, A. Efergan, N. Ohbayashi, M. Fukuda, D. Amihai, I. Hammel, M.E. Rothenberg, R. Sagi-Eisenberg, Rab5 is a novel regulator of mast cell secretory granules: impact on size, cargo, and exocytosis, J. Immunol. 192 (9) (2014) 4043–4053.
[39] S. Liu, M.N. Sahid, E. Takemasa, T. Kiyoi, M. Kuno, Y. Oshima, K. Maeyama, CRACM3 regulates the stability of non-excitable exocytotic vesicle fusion pores in a Ca(2+)-independent manner via molecular interaction with syntaxin4, Sci. Rep. 6 (2016) 28133.